Solid State Amorphization Reaction by Rod-Milling Al_xTa_<1-x> Powders and the Effect of Annealing

Sci. Rep. RITU A43 (1997) pp. 135-143
No. 2, March 1997

Solid State Amorphization Reaction by Rod-Milling Al_xTa_{1-x} Powders and the Effect of Annealing*

M. Sherif EL-ESKANDARANY[a,b], K. AOKI[c], K. SUMIYAMA[a], and K. SUZUKI[a]

[a]*Institute for Materials Research, Tohoku University, Sendai 980-77, Japan*
[b]*Permanent address: Mining and Petroleum Engineering Department, Faculty of Engineering, Al-Azhar University, Nasr City 11884, Cairo-Egypt*
[c]*Present address: Department of Materials Science, Kitami Institute of Technology, Kitami, Hokkaido 090, Japan*

(Received January 30, 1997)

High thermal stable amorphous Al_xTa_{1-x} alloy powders with wide amorphization range ($10 \leq x \leq 90$) have been synthesized by rod-milling technique using a mechanical alloying (MA) method. During the first few kiloseconds (11-173 ks) of the MA time, the layered-composite particles of Al and Ta are intermixed and form an amorphous phase upon heating at about 680 K in a differential thermal analyzer by thermally assisted solid state amorphization (TASSA). The heat formation of an amorphous Al_xTa_{1-x} alloy via the TASSA process, ΔH_{aT} has been measured as a function of the MA time. The crystallization characteristics indexed by the crystallization temperature, T_{xT} and the enthalpy of crystallization, ΔH_{xT} of the amorphous phase formed via the TASSA process are also investigated as a function of the MA time. Comparable with the TASSA process, a homogeneous amorphous Al_xTa_{1-x} alloy is formed after longer MA time (1080 ks). The amorphization process in this case is attributed to a mechanical solid state amorphization (MDSSA). At the end of the MA time (1080-1440 ks), the maximum heat of formation of an amorphous Al_xTa_{1-x} alloy via the MDSSA process, ΔH_{aM}, has been calculated. Moreover, the thermal stability characterized by the crystallization temperature, T_{xM} and the enthalpy of crystallization, ΔH_{xM}, are also estimated. The role of amorphization via each process has been discussed.

KEYWORDS: mechanical alloying, rod-milling, Al_xTa_{1-x} alloys, amorphization, crystallization

1. Introduction

The first report of a solid state amorphization reaction (SSAR)[1] via mechanical alloying (MA) process has been reported by Koch et al.[2] in 1983. Since then, many mechanically alloyed amorphous powders have been prepared using the ball milling[13-15] and/or the rod-milling[16-23] techniques. In addition, several metal nitrides[24-29], metal carbides[30-32] and metal hydrides[33,34] could be prepared at room temperature using the MA process.

In this work the rod-milling technique has been used for preparing composite powder particles containing mechanically-deformed multilayers of elemental Al and Ta powders. The influence of thermally-assisted-solid-state-reaction, TASSA[18,35] on the structure of these multilayered particles has been presented. Moreover, the progress of glass formation of Al_xTa_{1-x} alloy powders directly formed due to mechanically-solid-state-amorphization, MDSSA[36] via the MA process has been studied as well.

2. Experimental

Pure elemental Al (50 μm, 99.9%) and Ta (50 μm, 99.99%) powders were mixed to give the desired average composition of Al_xTa_{1-x} in a glove box under a purified argon atmosphere (O_2 and H_2O are less than 1 ppm) and sealed in a cylindrical stainless steel shell (SUS 304, 120 mm in diameter) together with ten stainless steel rods (SUS 304, 10 mm in diameter)[16]. The rod-to-powder weight ratio was about 30:1. The rod-milling was carried out at ambient temperature by mounting the rod-mill on a rotator at a rate of $1.4s^{-1}$. The MA experiments were interrupted at regular intervals and a small amount of the rod-milled powders was taken out from the vial in the glove box. The amorphization progress of the rod-milled powders was followed by means of X-ray diffraction (XRD) with MoKα and/or CuKα, differential thermal analysis (DTA) at a heating rate of 0.33 K/s and differential scanning calorimetry (DSC). All the DSC results presented in this study were obtained with heating rates of 0.67 K/s. The morphology of the alloyed powders was studied by scanning electron microscope/electron probe microanalyses (SEM/EPMA), using 30 kV microscope and transmission electron microscopy (TEM) using a 200 kV microscope. The induction coupled plasma (ICP) emission method was used to analyze the contents of Al and Ta, and the degree of Fe contamination in the milled powders. The oxygen contamination in the alloy powders was determined by the helium carrier fusion-thermal conductivity method.

*IMR, report No. 2071

3. Results

3.1. Structural change with the milling time

3.1.1. XRD

The total change in structure of rod-milled Al_xTa_{1-x} powders during the MA process was investigated by the X-

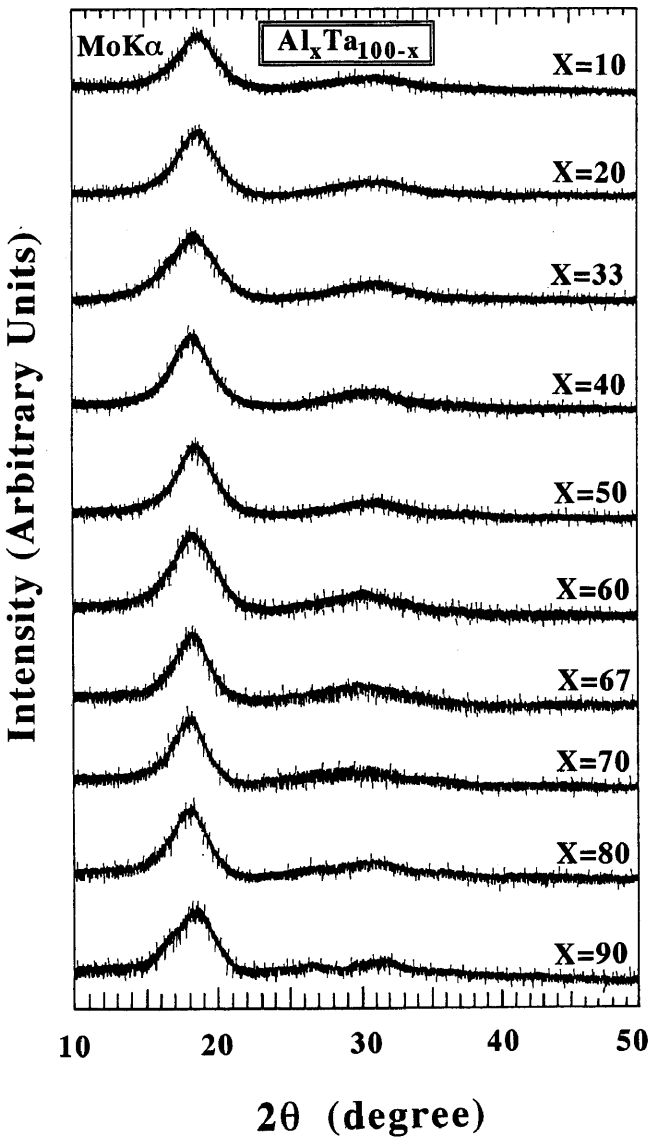

Figure 1. XRD patterns (using MoKα radiation) of rod-milled Al_xTa_{100-x} powders after 1440 ks of the MA time.

ray analyses. The XRD patterns (using MoKα radiation) of the end-product (1440 ks of the MA time) of Al_xTa_{1-x} powders are presented as a function of the atomic percent of Al content (x) in Fig. 1. Obviously, Al-Ta binary system possesses a wide amorphization range, extending from 10-90 at.% Al.

Figure 2 presents the correlation between the MA time and the powder's structural changes, taking $Al_{33}Ta_{67}$ alloy as a typical example. The XRD patterns at the initial stage of MA (0 ks) reveals sharp Bragg-peaks corresponding to fcc-Al and bcc-Ta crystals, as shown in Fig. 2(a). During the early stage of MA (0-86 ks) the Bragg-peaks for Al and Ta become wider and their intensities are decreased. During the intermediate stage of MA (86-360 ks) all the Bragg-peaks for Al crystals are surprisingly disappeared and the Bragg-peaks for Ta crystal become broader and their positions shifted remarkably to the low angle's side, indicating the formation of bcc solid solution, as presented in Figs. 2(e) and 2(f). The lattice parameter, a_0, of the powders after 256 ks of MA time has been calculated to be 0.3348 nm. This value is larger that of pure Ta crystal (0.3306 nm), suggesting an interstitial solubility of Al in Ta. Towards the end of this stage (360 ks) these peaks become broader with diffuse haloes, suggesting the formation of an amorphous coexisting with bcc solid solution, as illustrated in Fig. 2(g). At the final stage of MA (360-1440 ks) the bcc solid solution phase has been completely transformed to a homogeneous amorphous phase, characterized by diffuse and smooth peaks, as shown in Fig. 2(h) and 2(i).

3.1.2. TEM observations

The bright field image, BFI and the corresponding selected area diffraction pattern, SADP for rod-milled $Al_{33}Ta_{67}$ powders after 11 ks of the MA time are shown together in Fig. 3(a). Obviously, the sample is a mixture of polycrystalline Al and Ta. The powders at this stage of milling, have grain boundary fringes and dislocations in the boundary. The SADP shows sharp spot patterns related to fcc-Al crystals coexisting with bcc-Ta, as shown inset of Fig. 3(a).

The BFI and the corresponding SADP of the end-product $Al_{33}Ta_{67}$ powders (1440 ks of the MA time), are shown together in Fig. 3(b). Overall, the sample appears to have a homogeneous fine structure with no dominant facet structure. Moreover, the SADP shows a typical halo-pattern of an amorphous phase, being in a good agreement with the XRD patterns that presented in Fig. 2(h).

3.2. Morphology and metallography changes with the milling time

Figure 4 displays the correlation between the milling time, the particle size and the layer thickness of rod-milled $Al_{33}Ta_{67}$ powders at the different stages of MA. All the results presented Fig. 4 come from SEM and/or optical microscope observations. Obviously shown, the MA process can be classified into three stages, i.e., early or agglomeration, intermediate or disintegration and final or homogenization stages. At the early stage (0-86 ks) the alloying elements of Al and Ta powders are agglomerated and grow in their sizes as a result of the repeated cold welding. During this stage, the powders vary widely in size from 100 to about 600 μm. In parallel, the layer thickness of the particles are increased, as illustrated in Fig. 4. During the subsequent intermediate stage (86-360 ks), the agglomerated particles are subjected to a continuous disintegration with fragmentation to form finer powders with size less than 10 μm in diameter. Moreover, the layer thickness of the powder particles are dramatically decreased and hardly seen after 360 ks of the MA time, as shown in fig. 4. The final stage (360-1440 ks) refers to the last stage of MA in which all the particles are uniform in size (about 1 μm in diameter) without any morphological details.

3.3. Thermal stability

3.3.1. Amorphization process

The typical DTA curves of $Al_{33}Ta_{67}$ powders after selected MA time, are presented in Fig. 5. All the samples were heated up to 1400 K (first run) and cooled down to about 400 K. Then, second heating runs (dashed lines) were performed in order to establish the base line. After 4 ks there are two reactions. The first reaction that observed at about 900 K is an endothermic and occurs due to the melting of Al in the starting material of $Al_{33}Ta_{67}$ powders. The second reaction (exothermic) that centered at about 1200 K is attributed to a partial reaction of the unprocessed materials of Al and Ta powders. After 11 ks of the MA time, these reactions have already disappeared and the scan reveals two separate exothermic reactions. The peak

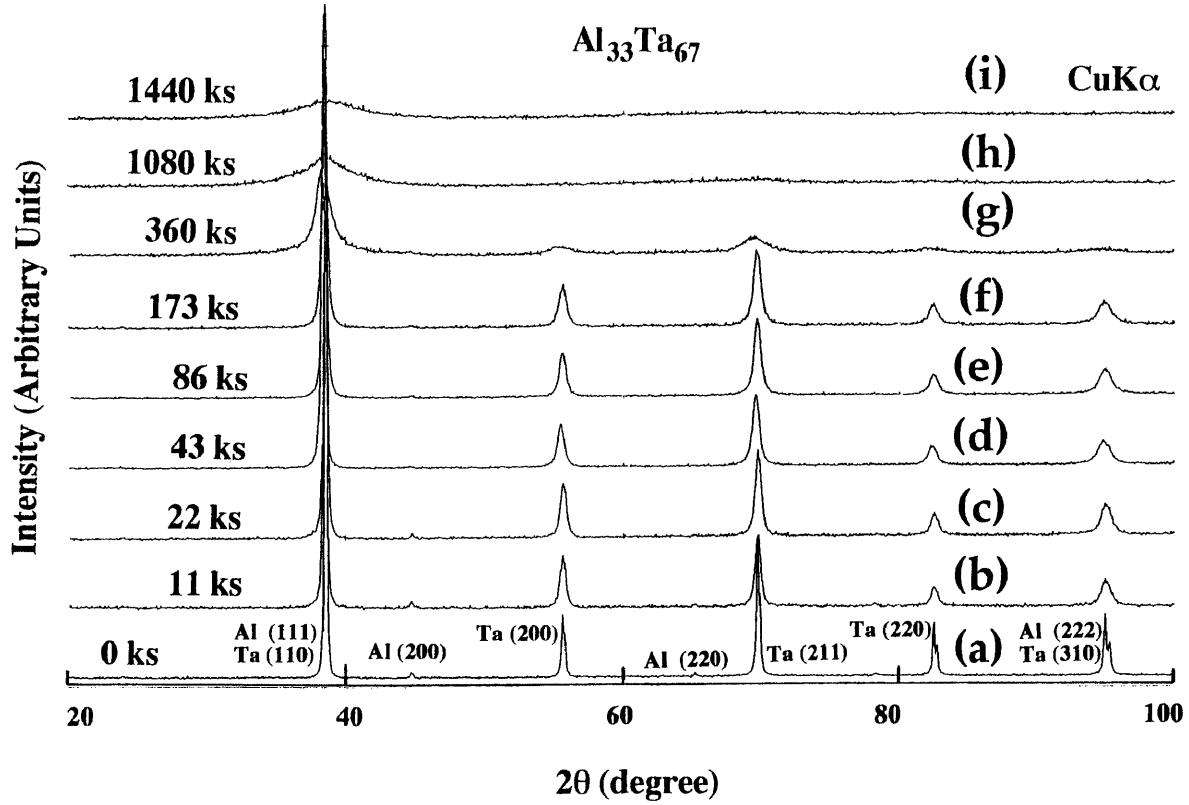

Figure 2. XRD patterns (using CuKα radiation) of rod-milled $Al_{33}Ta_{67}$ powders after selected MA times.

temperature of the first exothermic peak is independent on the MA time. Contrary to this, the peak temperature of the second exothermic peak is shifted to the elevated temperature during the early and the intermediate stages of milling, as displayed in Fig. 5. At the final stage of milling, the second exothermic peak becomes pronounced and sharp, while the first exothermic peak is surprisingly disappeared.

In order to understand the origin of these exothermic reactions, three samples of 86 ks alloy powders were heated separately in the DTA for TEM investigations at temperatures correspond to the points a, b and c in Fig. 5. The BFI's and the corresponding SADP's of the samples heated up to 500 K, 700 K and 1250 K are presented inset of Fig. 5. Sample (a) has layered-like morphology and the corresponding SADP from several regions shows rings-spot patterns that is characteristic of diffracting polycrystalline Al/Ta. Sample (b), however, indicates the formation of an amorphous phase, characterized by the fine and featureless image, and clear halo-pattern. Consequently, it is concluded that the first exothermic peak occurs due to a crystalline-to-amorphous phase transformation conducted by thermally assisted solid state amorphization, TASSA. Sample (c) shows at all regions without any exceptions cell or grain-like morphology with a sharp ring pattern. The ring pattern, which can be indexed as polycrystalline $AlTa_2$ (tetragonal structure) phase is characteristic of amorphous-to-crystalline phase transformation (crystallization process).

In the present study, the term ΔH_{aT} refers to the heat formation of the amorphous phase formed by TASSA and has been measures from the area under the amorphization peak, using the DSC analysis. Figure 6 shows the correlation between ΔH_{aT} and the MA time of rod-milled Al_xTa_{1-x} powders. In all compositions, ΔH_{aT} decreases drastically to approach minimum values and then increases dramatically to zero. Comparing with the powders in the Ta rich side (x=67), the Al-rich powders (X>50) the ΔH_{aT} appears after 22~43 ks and disappears after longer MA time (720 ks). This is attributed to the fact that the initial composite particles of Al_xTa_{1-x} in the Al-rich side contain very thick layers of metallic Al so that TASSA cannot be performed between such thick layers. Increasing the MA time leads to refinement of the layers and hence TASSA starts.

The heat formation of the amorphous phase formed by mechanically driven solid state amorphization, ΔH_{aM} is estimated during the final stage of milling (when the amorphization peaks are absent, i.e. $\Delta H_{aT} = 0$) using the following relation[37]:

$$\Delta H_{for} = \Delta H_a + \Delta H_x \quad (1)$$

Here, ΔH_{for} is the reported value of the enthalpy for formation an intermetallic compound at specific concentrations of Al based on Miedema's model[38] ΔH_a is the total heat of formation of amorphous phases formed by TASSA, ΔH_{aT} and MDSSA, ΔH_{aM} and ΔH_x is the total enthalpy change of crystallization for the amorphous phases caused by TASSA, ΔH_{xT} and MDSSA, ΔH_{xM}. Thus equation (1) can be written as follows:

$$\Delta H_{for} = (\Delta H_{aT} + \Delta H_{aM}) + (\Delta H_{xT} + \Delta H_{xM}) \quad (2)$$

During the final stage of milling (360-1440 ks) both ΔH_{aT} and ΔH_{xT} equal zero. Hence, equation (2) can be given as

$$\Delta H_{for} = \Delta H_{aM} + \Delta H_{xM} \quad (3)$$

The value of ΔH_{aM} can then be estimated from the

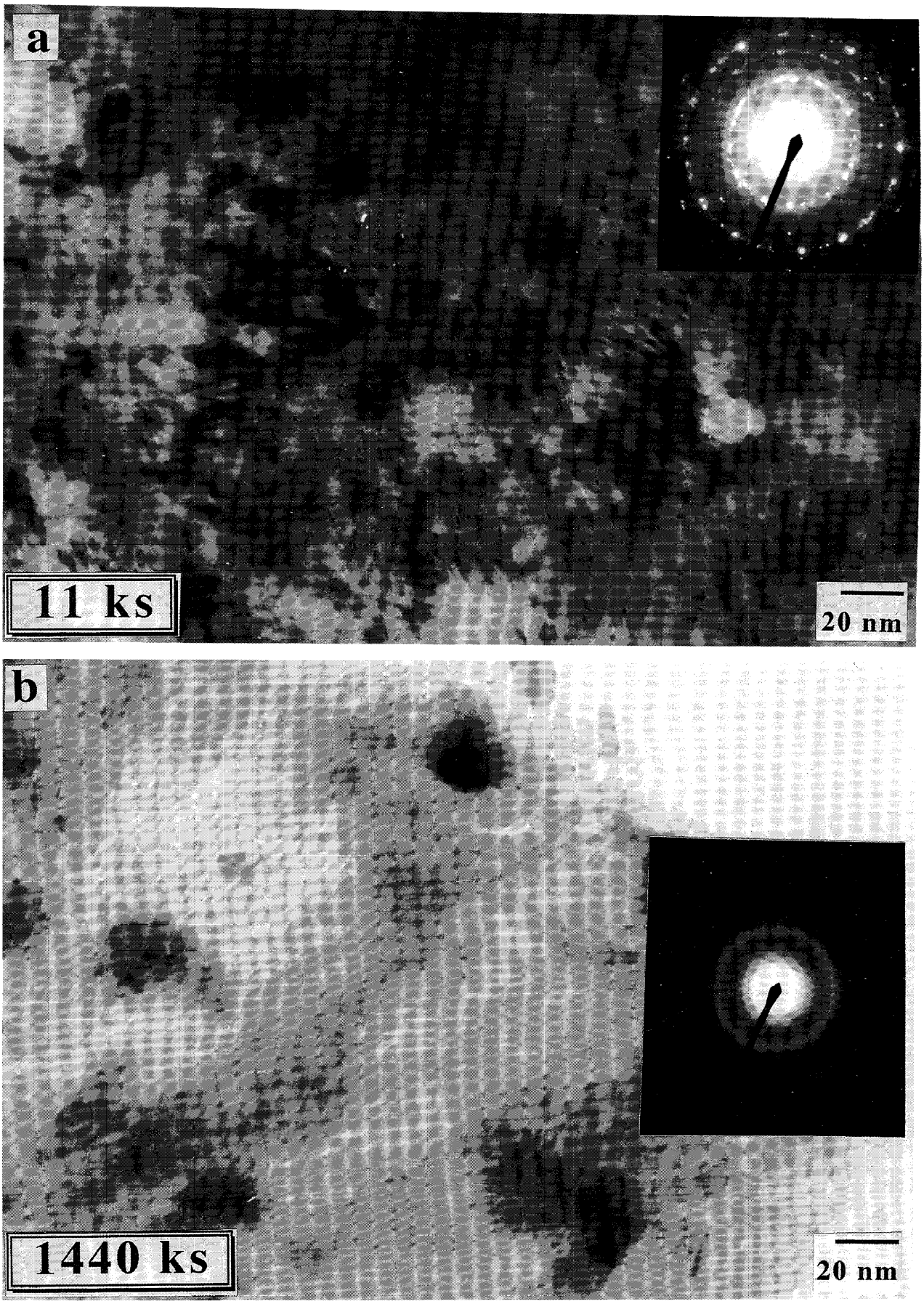

Figure 3. BFIs and the corresponding SADPs of rod-milled $Al_{33}Ta_{67}$ powders after (a) 11 ks and (b) 1440 ks of the MA time.

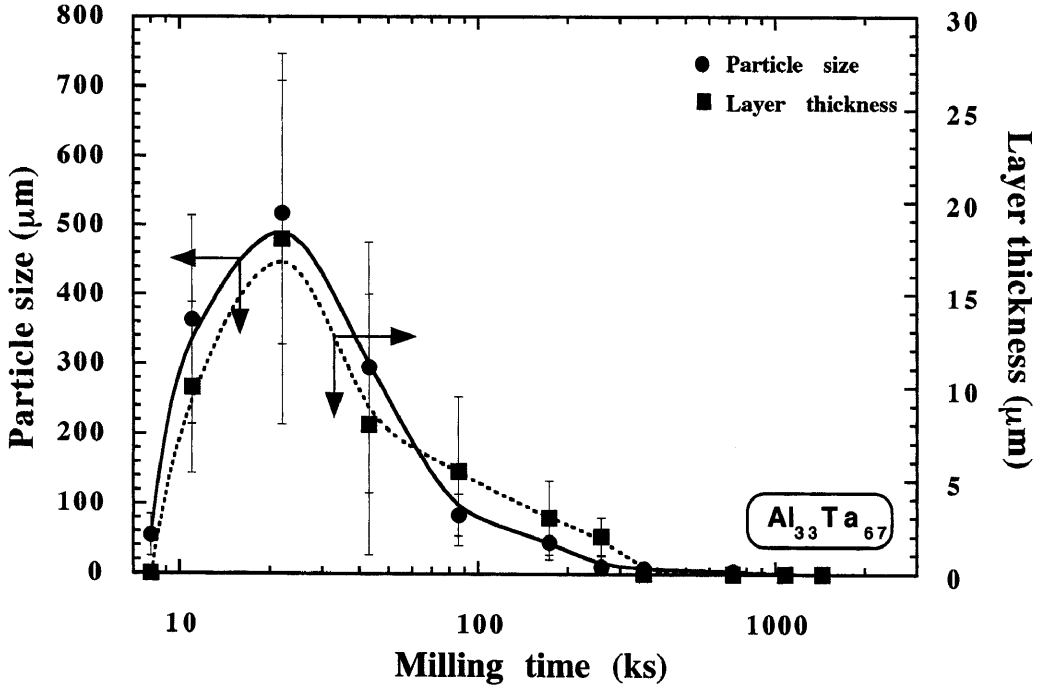

Figure 4. Correlation between the particle size (circles), layer thickness (squares) and the MA time of rod-milled $Al_{33}Ta_{67}$ powders.

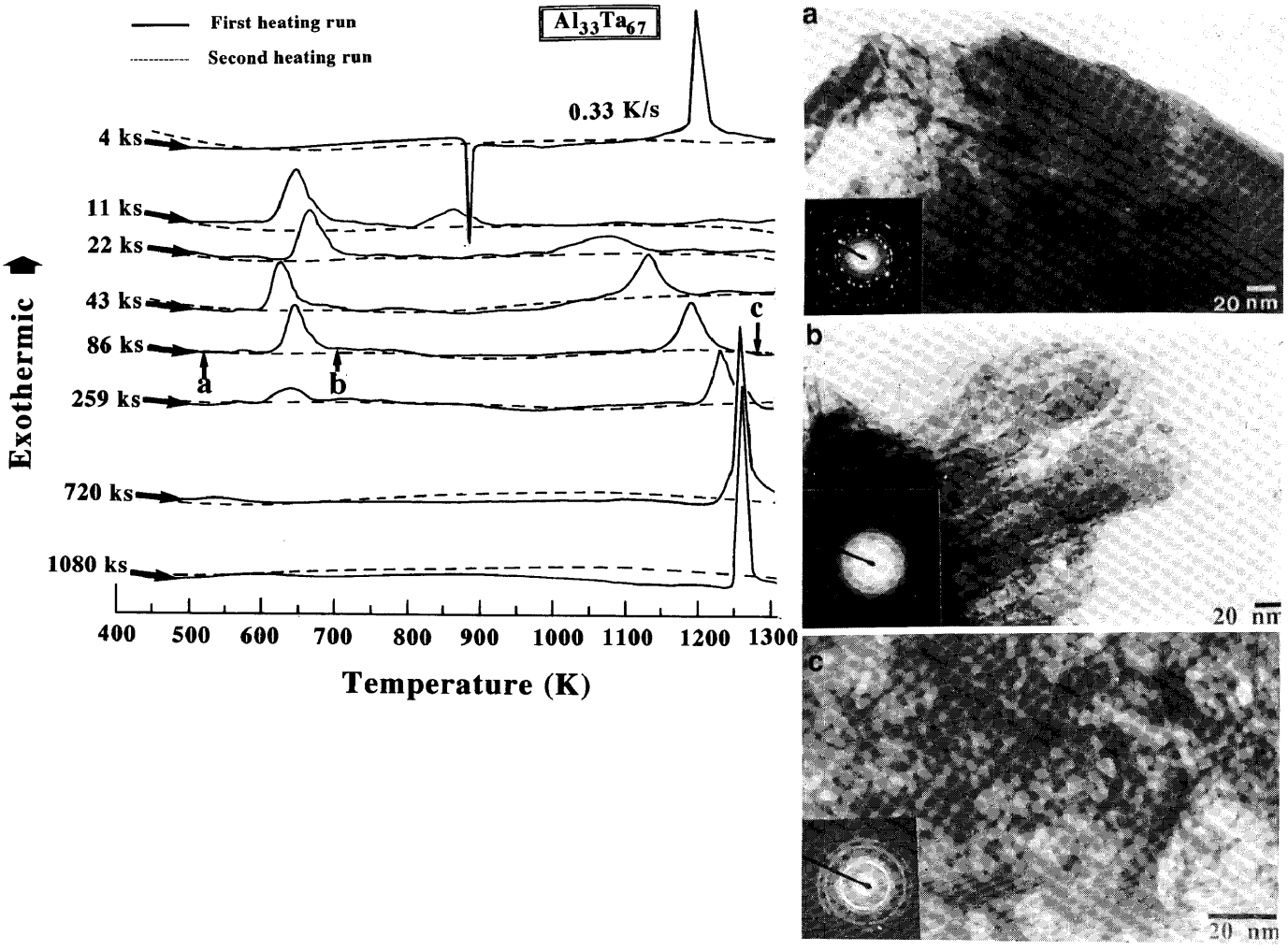

Figure 5. DTA traces associated with the amorphization reactions (low temperature peaks) and crystallization reactions (high temperature peaks) of rod-milled $Al_{33}Ta_{67}$ powders after selected MA time. The BFIs and the corresponding SADPs of 86 ks powders heated to (a) 500 K, (b) 800 K and (c) 1250 K are presented inset the figure.

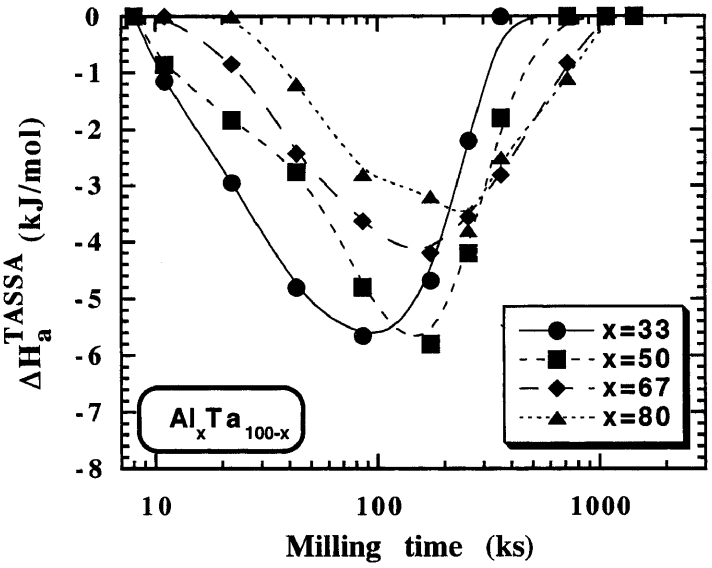

Figure 6. Dependence of the MA time and Al content (x) on the heat formation of amorphization via TASSA, ΔH_{aT} , of rod-milled Al_xTa_{1-x} powders.

following relation:

$$\Delta H_{aM} = \Delta H_{for} - \Delta H_{xM} \quad (4)$$

In fact, this value is very difficult to be estimated during the intermediate stage of milling (86-360 ks) which the measured value of ΔH_x is caused by the crystallization of the amorphous phases resulted from TASSA and MDSSA together.

3.3.2. Crystallization process

The crystallization characteristics of the amorphous powders indexed by the crystallization temperature, T_x, and the enthalpy change of crystallization, ΔH_x, are presented as a function of the MA time in Figs. 7(a) and 7(b) respectively. It can be seen in fig. 7(a) that the T_x of amorphous Al_xTa_{1-x} alloys increases monotonically during the early stage in which the amorphization process occurs only due to TASSA process. It then increases monotonically during the intermediate stage in which the amorphous phase(s) is formed due to the amorphization via TASSA and MDSSA together. This may suggest a gradual compositional change of the amorphous phase. During the last stage of milling, however, the amorphous phase is formed by MDSSA process only and the T_x approaches saturation value , indicating the completion of the amorphization process.

Further information of the crystallization reactions for Al_xTa_{1-x} alloy powders are given by ΔH_x (the total area under the crystallization peak), being the measure of the quantity of the amorphous fraction of the milled powders, is shown in Fig. 7(b). Between 11 and 86 ks of the MA time the value of ΔH_x decreases drastically, suggesting a rapid increasing in the volume fraction of the amorphous phase. Between 86 and 360 ks of the MA time, however, ΔH_x monotonically decreases, indicating a gradual increasing of the formed amorphous phase. After longer milling periods (720-1440 ks) ΔH_x tends to saturated values, indicating the formation of a homogeneous amorphous phase.

3.4. Chemical analysis

The contamination contents presented by the iron and oxygen of rod-milled $Al_{33}Ta_{67}$ alloy powders are presented as a function of the MA time in Fig. 8. During the early and the intermediate stages of milling, the iron contamination content (dotted line) that comes from the milling tool increases dramatically with the MA time to get a maximum value of 0.8 at.% after 360 ks of the MA time. During the final stage of milling the iron contamination content saturated a t a value of about 0.90 at.%.

The oxygen contamination content of the starting material of Al and Ta powders is about 0.25 at.%. However, the milling process and all of the measurements have been done in a high purified argon gas atmosphere, there is a monotonical increasing of the oxygen content of the alloy powders, specially during the early and the intermediate stages of milling. This may be attributed to the surface oxidation of the powder particles (that have fresh-active surfaces) during the materials handling outside the argon-glove box. The end-product of the alloy powders contains about 0.80 at.% of oxygen, as presented in Fig. 8.

4. Discussion

Amorphous Al_xTa_{1-x} alloy powders with wide amorphization range ($10< x < 90$) have been synthesized by TASSA and/or MDSSA process, using the rod-milling technique. In the TASSA process, the heat treatment of the composite powder particles containing well-developed structure of Al and Ta layers, enhances the solid state reaction between the diffusion couples. This leads to speed up the rate of diffusion at the clean Al/Ta boundaries so that the free energy changes drastically from a less stable (starting materials) to a more stable (amorphous) phases. In the MDSSA process, the solid state amorphization reaction (SSAR)[1] takes place in the same manner as occurs in the TASSA process, except with a lower diffusion rate and a long MA time. This is attributed to the milling temperature

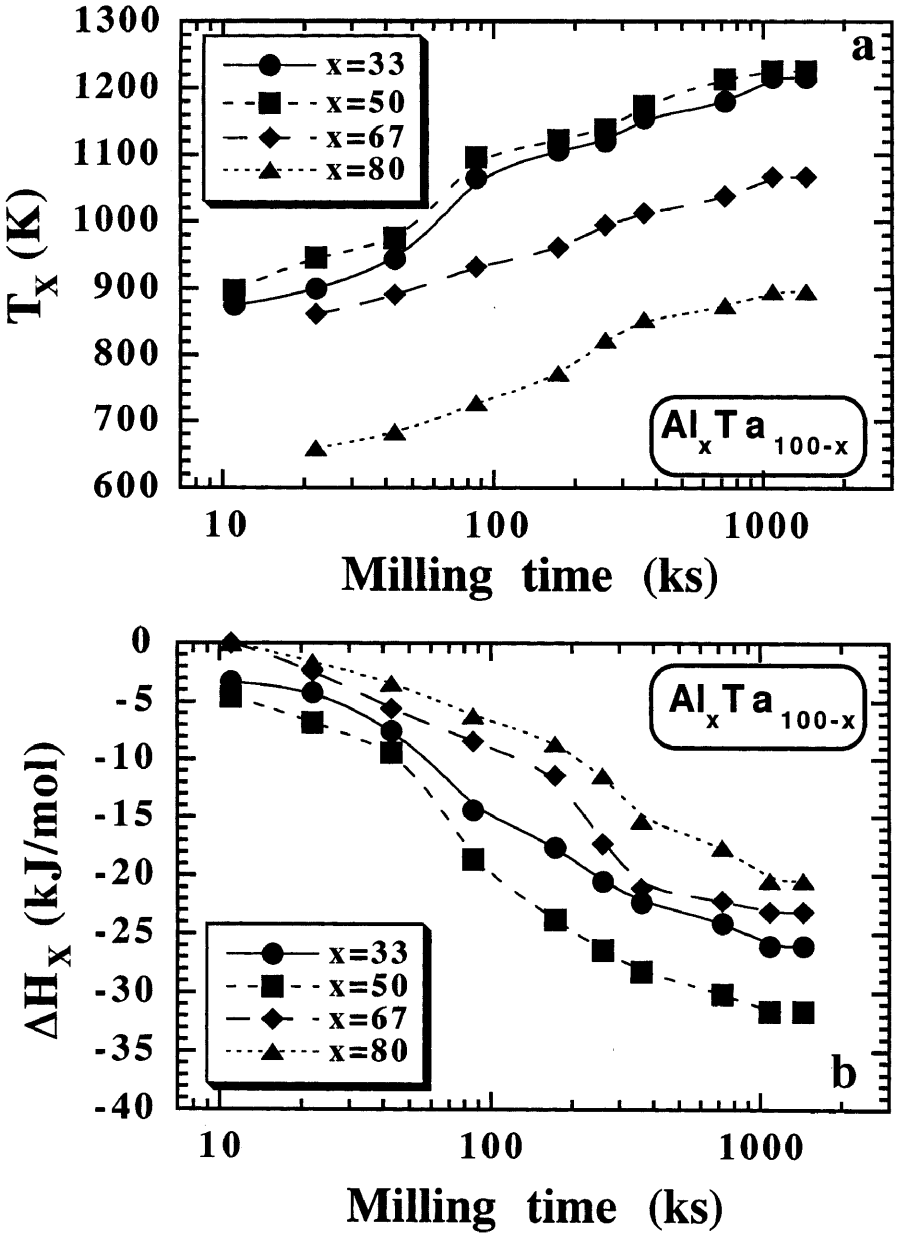

Figure 7. Effect of the MA time on the (a) crystallization temperature, T_x and (b) the enthalpy change of crystallization, ΔH_x of amorphous Al_xTa_{1-x} powders.

that is assumed to be far below that it is in TASSA (~ 680 K). Thus, the interdiffusion between Al and Ta layers occurs slowly. Although the two processes seem to be the same in appearance with a different time-scales, they produce amorphous alloys differ widely in thermal stability.

4. 1. The early stage of milling, the role of amorphization via TASSA process

This stage of milling (0-86 ks) refers to the first stage of MA in which the SSAR takes place only due to TASSA process. During the first few kiloseconds of this stage (0-22 ks), almost all the starting materials of Al and Ta are agglomerated to form powder particles containing many coarse layers of Al and Ta. Further milling (22-86 ks) leads to the formation of composite particles contain numerous narrow layers of metallic Al and Ta in a good arrangement as a result of the shear force generated by the rods[16]. This intensive shear force creates multilayered composite particles[35] that is typical of sputtered or evaporated diffusion couples. During the DTA measurements of the powder particles at this stage of milling, two separate exothermic peaks appear, as was shown in Fig. 5. The first exothermic reaction takes place at low temperature (about 680 K) and the second exothermic reaction occurs at higher temperature. The TEM image has led us to attribute the first peak to a complete SSAR in Al/Ta multilayers composite particles, while the second exothermic peak occured due to the crystallization of the yielded amorphous phase during the first reaction. This phenomena has been also shown in mechanically alloyed Ni-Ti[39], Al-Nb[19] and Al-Hf[35] binary systems. DSC allows measuring the enthalpy of amorphization via TASSA process, ΔH_{aT}, as presented in Fig. 6. As the thickness of Al and Ta layers in the composite particles decreases with increasing the MA time (Fig. 4), the number of these fresh layers increases. It is worth noting that this increasing of the layers plays a very important role for the amorphization via TASSA. The value of ΔH_{aT} increases drastically with increasing the number of these layers, suggesting a dramatic increasing in the volume

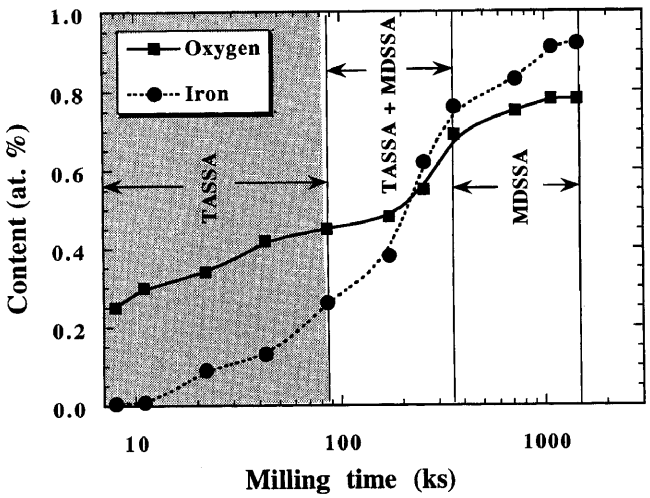

Figure 8. Influence of the MA time on the contamination presented by iron (triangle) and oxygen (circles) of rod-milled Al_xTa_{1-x} powders.

fraction of amorphous Al_xTa_{1-x} alloy powders. When the powder particles have no layered structure, heating them in the DTA does not lead to the formation of any amorphous phases, and then the value ΔH_{aT} becomes zero. During the TASSA process, both T_{xT} and ΔH_{xT} increase drastically, suggesting a dramatic compositional change[21] and an increase in the volume fraction of the amorphous phase[22] formed by TASSA process , as was presented in Figs. 7(a) and 7(b) respectively.

In fact, TASSA is an interesting process, in that an amorphous alloy can be obtained simply by heating the well-developed layered-composite particles to less that 700 K without further milling[17]. This process takes place in the same manner as SSAR in metallic multilayers thin films.

One advantage of TASSA process is to shorten the milling time and this leads to the formation of amorphous alloy with low contamination content, as illustrated in Fig. 8. However, the amorphous phase formed by TASSA process is rather heterogeneous, as suggested by the broadness of the crystallization peaks in Fig. 5. Moreover, this amorphous phase has low thermal stability, indicated by the low values of T_{xT} in Fig. 7(a).

4.2. The intermediate stage of milling, the role of amorphization via TASSA and MDSSA processes

In parallel to the TASSA process, a mechanical solid state amorphization reaction has been occurred at the fresh surfaces of the Al/Ta layers, with further milling time (86-360 ks). At the beginning of this stage, the Al atoms immigrate to Ta lattices to form bcc solid solution coexisted with unprocessed fcc-Al and bcc-Ta and an amorphous phase (that is mechanically formed). Here, the amorphization reaction takes place due to TASSA and MDSSA processes. During the progress of the milling at this stage, the number of layers are decreased (Fig. 4) so that ΔH_{aT} decreases dramatically, as was shown in Fig. 6. Since the amorphous phase of this stage of milling is formed mainly by MDSSA, the value of ΔH_{aM} is larger than ΔH_{aT}. Moreover, ΔH_{xM} is larger than ΔH_{xT}. This may give a sign that the effect of TASSA during this stage is gradually decreased. A complete bcc solid solution is yielded after 360 ks of MA time (Fig. 2), hence the layered-structure morphology has already disappeared. The disappearance of these layers eliminated the effect of TASSA process and ΔH_{xT} becomes zero at the end of this stage.

4. 3. The final stage of milling, the role of amorphization via MDSSA process

During this last stage of milling (360-1440 ks), the amorphization process occurs only due to the effect of MDSSA. A this stage, the several crystal imperfections such as points and lattice defects lead to a drastic change in the free energy of the end-product of the last stage. Thus, the solid solution phase (more stable phase) is transformed into a less stable phase (an amorphous phase) as was displayed in Fig. 2. At this stage of milling, the amorphous Al_xTa_{1-x} alloy powders are mechanically obtained without any heat treatments. Thus, both ΔH_{aT} and ΔH_{xT}.can be neglected. In fact, the amorphous Al_xTa_{1-x} alloy powders formed via MDSSA are very homogeneous and the presence of Al and/or Ta powders in the final-product could not be detected. Comparing with TASSA process, the amorphization via MDSSA process occurs fast and much more homogeneously. This is demonstrated by the nearly constant values of T_{xM} and ΔH_{xM} (see Fig. 7). One disadvantage of MDSSA process, is the long processing time which causes a rather high contamination with iron and oxygen, as was displayed in Fig. 8.

5. Conclusion

This is a study of the mode of amorphization and crystallization for mechanically alloyed Al_xTa_{1-x} powders using the rod-milling technique. The present study shows that an amorphous phase can be formed by two ways. The first way, that is called thermally assisted solid state amorphization, TASSA, takes place in the mechanically-deformed Al/Ta composite particles by heating the milled powders around 680 K in an argon atmosphere. In the second way, however, an amorphous phase is formed directly after long milling time due to mechanically driven solid state amorphization, MDSSA. The heat formation of amorphization and crystallization via each process has been estimated.

Acknowledgments

This work was partially supported by a Grant-in-Aid for Co-operative Research (07305033), given by the Ministry of Education, Science, Sports and Culture, Japan.

1) R. B. Schwarz and W. L. Johnson, Phys. Rev. Lett. **51**, (1983) 415.
2) C. C. Koch, O. B. Cavin, C. G. MacKamey and J. O. Scarbourgh, Appl. Phys. Lett. **43**, (1983) 1017.
3) C. Politis and W. L. Johnson, J. Appl. Phys. **60**, (1986)1147 .
4) R. Schwarz and C. C. Koch, Appl. Phys. Lett. **49**, (1986) 146.
5) P. Y. Lee and C. C. Koch, J. Non-Cryst. Solids **94**, (1987) 88.
6) E. Hellstern and L. Schultz, J. Appl. Phys. **63**, (1988) 1408.

7) K. Suzuki, J. Non-Cryst. Solids **112**, (1989) 23.
8) E. Gaffet and M. Harmelin, J. Less-Common Met. **157**, (1990) 201.
9) J. S. C. Jang and C. C. Koch, J. Mater. Res. **5**, (1990) 498 .
10) M. Sherif El-Eskandarany, F. Itoh, K. Aoki and K. Suzuki, J. Non-Cryst. Solids **117/118**, (1990) 729.
11) R. B. Schwarz, S. Srinivasan and P. B. Desch, Mater. Sci. Forum **88-90**, (1992) 595.
12) P. Nash, H. Kim, H. Choo, H. Ardy, S. J. Hwang and A. S. Nash, Mater. Sci. Forum **88-90**, (1992) 603.
13) J. Eckert, Mater. Sci. Forum **88-90**, (1992) 679.
14) E. Gaffet, N. Malhouroux and M. Abdellaoui, J. Alloys Comp. **194**, (1993) 339.
15) K.-J. Kim, M. Sherif El-Eskandarany, K. Sumiyama and K. Suzuki, J. Non-Cryst. Solids **155**, (1993) 165.
16) M. Sherif El-Eskandarany, K. Aoki and K. Suzuki, J. Less-Common Met. **167**, (1990) 113.
17) M. Sherif El-Eskandarany, K. Aoki and K. Suzuki, Scripta Metall. **25**, (1991) 1695.
18) M. Sherif El-Eskandarany, K. Aoki and K. Suzuki, J. Alloys Comp. **177**, (1991) 229.
19) M. Sherif El-Eskandarany, K. Aoki and K. Suzuki, J. Appl. Phys. **72**, (1992) 2665.
20) M. Sherif El-Eskandarany, K. Aoki and K. Suzuki, Mater. Sci Forum **88-90**, (1992) 81.
21) M. Sherif El-Eskandarany, K. Aoki and K. Suzuki, Met. Trans. A **23**, (1992) 2131.
22) M. Sherif El-Eskandarany, K. Aoki and K. Suzuki, J. Appl. Phys. **71**, (1992) 2924 .
23) M. Sherif El-Eskandarany, K. Aoki and K. Suzuki, J. Non-Cryst. Solids **150**, (1992) 472 .
24) M. Sherif El-Eskandarany, K. Sumiyama, K. Aoki and K. Suzuki, Mater. Sci. Forum **88-90**, (1992) 801.
25) M. Sherif El-Eskandarany, K. Aoki and K. Suzuki, Appl. Phys. Lett. **60**, (1992) 1562.
26) M. Sherif El-Eskandarany, K. Sumiyama, K. Aoki and K. Suzuki, J. Mater. Res. **7**, (1993) 888.
27) K. Aoki, A. Memezawa and T. Masumoto, J. Mater. Res. **8**, (1993) 307.
28) M. Sherif El-Eskandarany, J. Alloys Comp. **203**, (1994) 117.
29) M. Sherif El-Eskandarany, K. Sumiyama, K. Aoki, T. Masumoto and K. Suzuki, J. Mater. Res. **9**, (1994) 2891.
30) T. Tanaka, K. N. Ishihara and P. H. Shingu, Met. Trans. A **23**, (1992) 2431.
31) M. Sherif El-Eskandarany, K. Sumiyama and K. Suzuki, J. Mater. Res. **10**, (1995) 659.
32) M. Sherif El-Eskandarany, Met. Trans. A **27** (1996) 1996.
33) K. Aoki, A. Memezawa and T. Masumoto, J. Mater. Res. **9**, (1994) 39.
34) M. Sherif El-Eskandarany, H. A. Ahmed, K. Sumiyama and K. Suzuki, J. Alloys Comp. **218**, (1995) 36.
35) M. Sherif El-Eskandarany, K. Aoki, T. Masumoto and K. Suzuki, J. Alloys comp. **209**, (1994) 71.
36) M. Sherif El-Eskandarany, J. Alloys Comp. **234 / 1**, 67 (1996) 1996.
37) M. P. Henaff, C. Colinet, A. Pasturel and K. H. J. Buschow, J. Appl. Phys. **56**, 307 (1984).
38) A. R. Miedema, J. Less-Common Metals **32**, (1973) 117.
39) R. B. Schwarz and R. R. Petrich, J. Less-Common Metals **140**, (1988) 171.